Crystal structure of the deglycating enzyme Amadoriase I in its free form and substrate-bound complex

Federica Rigoldi,[1] Alfonso Gautieri,[1] Andrea Dalle Vedove,[2,3] Anna Paola Lucarelli,[2] Simone Vesentini,[1] and Emilio Parisini[2]*

[1] Dipartimento Di Elettronica, Informazione E Bioingegneria, Politecnico Di Milano, Milano, 20133, Italy

[2] Center for Nano Science and Technology @Polimi, Istituto Italiano Di Tecnologia, Milano, 20133, Italy

[3] Dipartimento Di Chimica, Materiali E Ingegneria Chimica "G. Natta", Politecnico Di Milano, Milano, 20133, Italy

ABSTRACT

Amadoriases, also known as fructosyl amine oxidases (FAOX), are enzymes that catalyze the de-glycosylation of fructosyl amino acids. As such, they are excellent candidates for the development of enzyme-based diagnostic and therapeutic tools against age- and diabetes-induced protein glycation. However, mostly because of the lack of a complete structural characterization of the different members of the family, the molecular bases of their substrate specificity have yet to be fully understood. The high resolution crystal structures of the free and the substrate-bound form of Amadoriase I shown herein allow for the identification of key structural features that account for the diverse substrate specificity shown by this class of enzymes. This is of particular importance in the context of the rather limited and partially incomplete structural information that has so far been available in the literature on the members of the FAOX family. Moreover, using molecular dynamics simulations, we describe the tunnel conformation and the free energy profile experienced by the ligand in going from bulk water to the catalytic cavity, showing the presence of four gating helices/loops, followed by an "L-shaped" narrow cavity. In summary, the tridimensional architecture of Amadoriase I presented herein provides a reference structural framework for the design of novel enzymes for diabetes monitoring and protein deglycation.

Key words: deglycating enzyme; enzyme structure; molecular modeling; protein crystallization; glycation.

INTRODUCTION

There is extensive clinical data in the literature on age- and diabetes-related alterations in the functioning of all human tissues, including susceptibility to injury and reduced healing capacity.[1] Tissue aging is characterized by a progressive accumulation of advanced glycation end-products (AGEs) especially in collagen-rich tissues, owing to the low turnover of this structural protein.[2] Besides the elderly, people who suffer from type II diabetes are particularly affected by AGEs accumulation: whilst elder people have abundance of long-lived proteins that have slowly accumulated AGEs over time, type II diabetics have abnormally high levels of glucose in their blood, a surplus that can readily glycate proteins.[3,4] The glycation reaction is spontaneous and initiates with the formation of a reversible Schiff base between a carbohydrate, typically glucose, and a protein amino group (for example, the lysine side-chain). The unstable Schiff base becomes a stable intermediate keto-amine, commonly referred to as Amadori product. Then, over time (usually months or years), a complex series of reactions leads to

Abbreviations: AGEs, advanced glycation end-products; CVs, collective variables; FAODs, fructosyl amino acid oxidases; FAOX, fructosyl amine oxidases; FEP, free energy perturbation; FLY, fructosyl-lysine; FSA, fructosyl-thyoacetate; GAFF, general amber force field; OPD, o-phenylenediamine; RAMD, random acceleration molecular dynamics

Grant sponsor: Fondazione Cariplo; Grant numbers: 2013–0766, 2011-0270; Grant sponsor: European Union; Grant number: "Marie Curie" FP7 IRG N. 268231; Grant sponsor: Istituto Italiano di Tecnologia.

Federica Rigoldi and Alfonso Gautieri contributed equally to this work.

*Correspondence to: Emilio Parisini, Center for Nano Science and Technology @Polimi, Istituto Italiano di Tecnologia, Via G. Pascoli 70/3, 20133 Milano, Italy. E-mail: Emilio.Parisini@iit.it

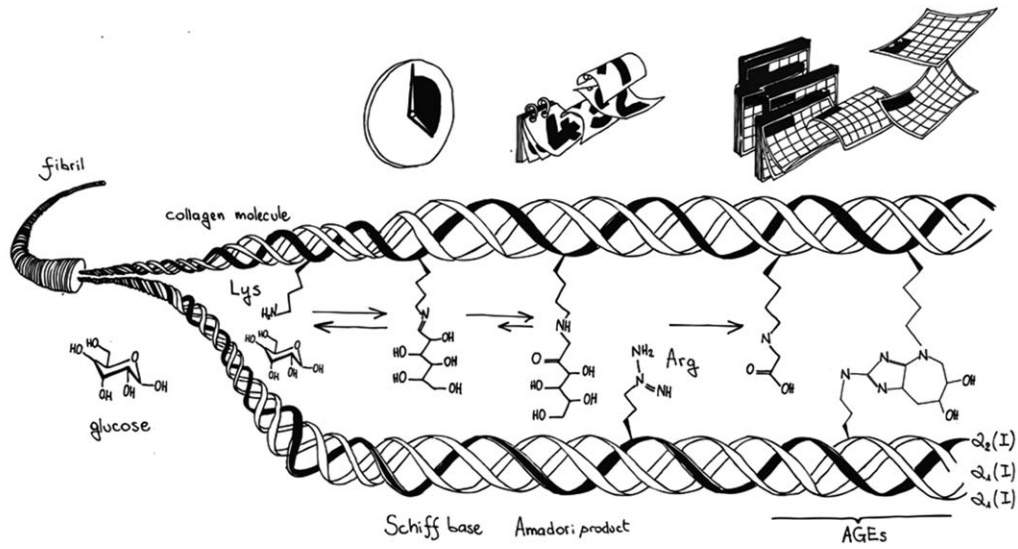

Figure 1

Schematic of the protein glycation pathway *in vivo*, from left to right. A free amine (for example, lysine side chain) reacts with the aldehyde group of circulating glucose producing an unstable Schiff base. This compound is stabilized through Amadori rearrangement, resulting in a stable product. Over the course of months or years, the Amadori product can then undergo multiple rearrangements that lead to several different AGEs. In particular, AGEs crosslinks are formed in the presence of a reactive group from a nearby protein. In the picture, the side-chain of a nearby arginine leads to the formation of pentosidine, a fluorescent crosslinking AGE.

the formation of several types of AGEs, which can be either adducts or crosslinks[5] (Fig. 1).

The hyperglycemia associated with diabetes results in the non-enzymatic glycation of blood proteins. For this reason, the measurement of the levels of glycated hemoglobin (HbA1c) in the blood is a very powerful method for monitoring the insurgence and development of diabetes. Indeed, while the direct blood sugar level measurement is affected by daily fluctuations, the long lifetime of hemoglobin combined with the slow, yet irreversible, glycation process makes the detection of HbA1c a good indicator of the average blood glucose concentration over a period of 2–3 months. Several systems have been developed that are used in the clinics to measure HbA1c[6]; however, they are based on relatively complex and expensive techniques such as chromatography and electrophoresis. Hence, there is a need for fast and easy HbA1c detection, possibly to be performed at home or at a point of care.

Amadoriases, also known as fructosyl amino acid oxidases (FAODs) or fructosyl amine oxidases (FAOX)[7–9] are enzymes that are found in fungi and bacteria and that are able to cleave low molecular weight Amadori product (i.e, glycated amino acids) to yield a free amine, glucosone, and hydrogen peroxide.[10,11] These enzymes have been categorized[12] into three groups depending on their substrate specificity. Group I FAOX are active mostly on α-fructosyl amino acids (that is, amino acids glycated on backbone amines), group II FAOX are active mostly on ϵ-fructosyl amino acids (that is, amino acids glycated on side-chain amines), while group III FAOX show similar activity on either α- or ϵ-fructosyl amino acids. The development of Amadoriase-based sensors is wildly regarded as a promising approach to meet the need for a fast and simple HbA1c monitoring method. An important issue for these sensors is that enzymatic HbA1c sensing relies on the specific detection of the glycated N-terminal valine. However, wild-type Amadoriases are unspecific for valines since they also cleave glycated lysines that are present on haemoglobin, which therefore interfere with the measurement of HbAc1. A second major limitation is the fact that available Amadoriases are inactive on intact, wild-type haemoglobin. Therefore, enzyme-based HbA1c sensors require a preliminary proteolytic digestion of the protein to release the N-terminal valine residue, a step that increases the time and the complexity of the sensing method.

Glycation and AGES are also associated to several deleterious effects: on one hand, they alter molecular recognition by modifying the biochemistry of protein binding sites,[13,14] on the other hand AGEs crosslinks such as glucosepane can alter the mechanical properties of load bearing proteins, such as collagen, leading to stiffer tissues.[15–17] However, to date, there are no effective ways to prevent or eliminate AGEs, except reducing the dietary sugar intake.[18] The use of enzymes from either the Amadoriase family or from the fructosyl amino acids kinases family has been proposed as a promising strategy for protein deglycation to restore properties and function in glycated proteins in our body[7,8] or in food products.[19]

Fructosamine kinases are active in the intracellular environment, they need ATP as energy source and they produce 3-deoxiglucosone, which is a toxic compound that would need removal.[20]

Amadoriases, on the other hand, appear to hold more promise as a protein deglycation tool since they work in the extracellular environment, do not need ATP, and do not produce toxic chemicals. However, despite the fact that from the first isolation of an Amadoriase enzyme[21] over a dozen similar enzymes have been reported in the literature,[12] none has shown significant activity on intact proteins, even after extensive mutagenesis experiments.[22,23]

These two remarkable potential applications of Amadoriases highlight the need for the precise knowledge of the overall folding architecture and active site conformation of the different FAOX family members. The lack of such crucial piece of information has so far been one of the major limiting factors for the development of novel Amadoriase-like enzymes for diagnostic or therapeutic applications. This structural limit has been overcome in part by the successful determination of the free and the inhibitor-bound crystal structures of Amadoriase II from *Aspergillus fumigatus,*[24] and by the more recent structure of the free fructosyl peptide oxidase from *Eupenicillium terrenum* (known as FPOX-E or EtFPOD)[25] which, to date, are the only known FAOX structures available in the literature. However, Amadoriase II has been reported to be mostly active on backbone fructosyl amines[12,26] and on hydrophobic substrates (for example, glycated glycines),[24] whereas FPOX-E is active mostly on α-fructosyl amino acids.[12,24]

In this work, we show the first crystal structures of a group II FAOX, namely the free and the substrate-bound form of the isoenzyme Amadoriase I from *Aspergillus fumigatus*, both at high resolution. This enzyme is a promising candidate for protein deglycation as it is mostly active on side-chain fructosyl amines and on charged substrates (for example, glycated lysines), which are similar to the Amadori product that *in vivo* lead to AGEs. Furthermore, the details provided for the first time on the active site conformation of a group II Amadoriase can help the development of novel enzymes with improved catalytic specificity for diagnostic applications.

MATERIALS AND METHODS

Protein expression and purification

The DNA gene sequence coding for Amadoriase I protein was fused at its N terminus to an initial Met residue, a 6His-tag, a spacer region of five amino acid residues (Ser-Ser-Gly-His-Ile) and the enterokinase recognition site (Asp-Asp-Asp-Asp-Lys). The sequence, cloned into the pET3a vector (Novagen) using the NdeI and BlpI cloning sites, was synthetized by Eurofins MWG. *E. coli* BL21(DE3)pLysS cells (Invitrogen) were then transformed with the resulting clone and grown in LB medium supplemented with 100 mg/liter ampicillin (Sigma). Cells were grown at 37°C until $A_{600} = 0.6$ was reached and expression was induced by adding isopropyl 1-thio-β-D-galactopyranoside (Sigma) to a final concentration of 0.5 m*M*. Subsequent overnight protein expression at 25°C provided soluble protein in very high yield. The cell lysate was then purified by nickel affinity chromatography. A second and final purification step using a Hiprep 26/60 Sephacryl S-100 size exclusion column (GE Healthcare) was performed in order to obtain 100% sample purity as detected by Coomassie staining. Absorbance at 450 nm was monitored to identify the fractions with the most intense yellow color. The fractions of this last affinity chromatography step were collected, dialyzed into 10 m*M* Tris buffer pH 8.0, and brought to a final concentration of 15 mg/mL for crystallization experiments.

Protein crystallization

Crystals of the free form of Amadoriase I from *Aspergillus fumigatus* were obtained by vapor diffusion at room temperature by mixing a 1 μL drop of the protein sample with an equal volume of a solution containing 0.1*M* sodium citrate pH 5.6, 10% PEG4K, 15% isopropanol. Crystals were then frozen in a chemically identical solution to which 25% (v/v) glycerol was added to serve as cryo-protectant for X-ray data collection. Crystals of the substrate-bound form of the same enzyme were obtained by co-crystallization, mixing a 1 μL drop of Amadoriase I (15 mg/ml, 300 μM) with 1 μL drop of ligand (3 mg/mL, 10 m*M*), and 1 μL drop of the same crystallization buffer used for the free form (0.1*M* sodium citrate pH 5.6, 10% PEG4K, 15% isopropanol). Crystallization experiments were set up in anaerobic conditions using a glove box in order to prevent oxidase activity. The ligand, N^{ϵ}-fructosyl-lysine (FLY), was kindly provided by researchers S.M. Monti, G. Roviello (Institute of Biostructures and Bioimaging of the National Research Council, Italy) and V. Fogliano (Wageningen University, The Netherlands), and produced as described previously.[27,28]

Structure determination and refinement

A 1.6 Å (free form) and a 1.9 Å (substrate-bound form) resolution data set were collected from single Amadoriase I crystals using $\lambda = 1.000$ Å in the X06DA-PXIII beamline at the Swiss Light Source (Paul Scherrer Institute, Villigen, Switzerland). Diffraction images were processed and scaled using XDS (Kabsch-2010). Data collection and refinement statistics are shown in Table I. The first of the two structures (the free form) was determined by molecular replacement using MOLREP[29] from the CCP4 package[30] and the free Amadoriase II structure

Table I
Data Collection and Refinement Statistics of the Free and the Substrate-Bound Amadoriase I Enzyme Structures

Crystal	Amadoriase I, free (PBD id: 4WCT)	Amadoriase I, bound (PBD id: 4XWZ)
Data collection		
Space group	$P2_12_12_1$	$P2_12_12_1$
Cell dimensions		
a (Å)	70.3	70.2
b (Å)	83.1	83.2
c (Å)	176.8	176.1
Wavelength (Å)	1	1
Resolution (Å)	48.07–1.67	47.96–1.90
R_{sym} or R_{merge} *(%)*	7.9 (47.3)	11.7 (73.6)
$I/\sigma I$	28.94 (4.06)	12.8 (2.6)
Completeness (%)	98.85 (93.01)	99.3 (95.7)
Multiplicity	5.6	7.3
Refinement		
Resolution (Å)	48.07–1.67	47.96–1.90
No. of reflections	119826	77606
R_{work}/R_{free} *(%)*	13.9/16.9	14.9/18.5
No.of atoms:		
Protein	7004	6922
Ligand:FAD-FLY	106 (FAD)	106 (FAD)–42 (FLY)
Water	1184	660
Average B-factors (Å^2):		
Protein	15.50	24.22
Ligand	8.90 (FAD)	16.21(FAD)–53.86 (FLY)
Water	29.7	34.83
r.m.s.d		
Bond lengths (Å)	0.005	0.003
Bond angles (°)	0.984	0.676
Ramachandran:		
Most favored(%)	98	96.5
Additional allowed (%)	2	3.5
Disallowed (%)	0	0

(PDB code: 3DJD) as the search probe, while the second (the substrate-bound form) was refined starting from our free Amadoriase I structure.

In both cases, model building and refinement were carried out using REFMAC5[31] and PHENIX.[32] The library for the refinement of the ligand and the cofactor portions of the structures was built using the JLigand tool in the CCP4 package. Water molecules were added both automatically using the phenix_refine tool from the PHENIX package and manually from visual inspection of the electron density map. All the figures in the article were generated using PyMOL (http://www.pymol.org) or VMD.[33] The refinement of the two structures converged to a final $R/R_{free} = 13.9/16.9\%$ (free form) and $R/R_{free} = 14.9/18.5\%$ (substrate-bound form).

Classical molecular dynamics simulations

We used our high resolution crystal structures of the free and the substrate-bound form of Amadoriase I (PDB code: 4WCT and 4XWZ) to carry out extensive molecular dynamics (MD) simulations and study the enzyme-substrate dynamic interactions, binding free-energy, tunnel conformations and egress trajectory. The analysis of the dynamic interactions of fructosyl-lysine within the binding pocket was done by means of a 1 μs molecular dynamics simulation in explicit solvent using the FLY-bound Amadoriase I crystal structure (PDB entry: 4XWZ) as the input model. The protein was modelled using the AMBER99SBildn force field[34] while the FAD co-factor and ligand were modelled using the general amber force field (GAFF).[35] The complex was then solvated with 14,992 TIP3P water molecules and neutralized with the addition of 37 Cl^- ions and 47 Na^+ ions. The setup resulted in a system of 52,003 atoms in a simulation box of initial dimensions $82 \times 76 \times 95$ Å^3.

The system was minimized and equilibrated using the NAMD code[36] under constant pressure and temperature (NPT) conditions in order to relax the volume of the periodic box. The pressure was set to 1 atm and the temperature to 300 K, while using a time step of 2 fs, a non-bonded cut-off of 9 Å, rigid bonds and particle-mesh Ewald long-range electrostatics. During minimization and NPT equilibration, the C_α atoms of the protein were restrained by a 10 kcal mol $^{-1}$ Å $^{-2}$ spring constant to prevent protein diffusion. Finally, the production run was performed using ACEMD[37] on a NVIDIA GeForce GT 640 GPU for a total time of 1 μs. A longer time step of 4 fs was used thanks to the use of the hydrogen mass repartitioning scheme implemented in ACEMD. All other parameters (temperature, non-bonded cut-off, and PME) were kept the same as in the equilibration phase. In order to avoid protein diffusion, an harmonic restraint of 1 kcal mol^{-1}Å^{-2} was applied on C_α atoms of the protein farther than 20 Å from the binding pocket. The stability of the system was checked by monitoring the convergence of the root mean square deviation (r.m.s.d.) of the protein. H-bonds between the protein and the substrate were calculated using tcl-scripts[38,39] in VMD[33] on a geometric basis (donor-acceptor distance < 3 Åand donor-hydrogen-acceptor angle $< 20°$).

Tunnel conformation and egress trajectory

We used the CAVER 3.0.1[40] program to calculate the pathway leading from the buried active site to the bulk solvent. For the analysis of the geometry of the tunnel we used 20 snapshots from the equilibrated production MD run. The ligand, ions and water molecules included in the MD runs were removed during tunnel calculation. The substrate position within the active site as seen in our crystal structure was used as the starting point. We chose a probe consisting of a sphere with a 1.5 Å radius to account for the bulky sugar ring of the ligand.

We compared the results of the tunnel calculation with the egress pathway determined using the random acceleration molecular dynamics (RAMD)[41] simulation technique, which has been developed to identify egress routes for a ligand from a buried protein binding site. RAMD simulations of the complex between Amadoriase I and

fructosyl-lysine were performed with the NAMD code and the RAMD 4.1 tcl script.

We chose 10 starting configurations for the RAMD simulations from the production MD run. The maximum duration of each RAMD simulation was set to 1 ns; when a ligand exit event was detected, i.e. the distance between the fructosyl-lysine center of mass and the Amadoriase I center of mass exceeded 35 Å, the simulation was halted. The RAMD parameters used were as follows: acceleration of 0.25 kcal $mol^{-1}Å^{-1}$ amu^{-1}, force direction re-evaluation every 100 steps and distance threshold of 0.4 Å.

Metadynamics calculations

We used well-tempered metadynamics simulations[42] to estimate the free energy profile of ligand exit from the Amadoriase I cavity. Calculations were done using the PLUMED 1.3 plugin[43] together with ACEMD software[37] and run in NVT ensemble at a temperature of 300 K for 400 ns. We used two separate collective variables (CVs) to describe the ligand exit. The first CV was defined as the distance between the lysine N^{ϵ} moiety and the FAD N(5) atom (CV1, monitored in the range 2.5–20 Å), accounting for the distance between the ligand and the binding pocket. The second CV was defined as the angle between the lysine N^{ϵ}, the C(1) atom of the sugar ring and the FAD N(5) atom (CV2, range 0°–180°), which accounts for the orientation of the ligand with respect to FAD. Preliminary tests have shown that because of the elongated shape of the ligand, a single CV would not be sufficient to properly describe the free energy profile. The Gaussian potentials were added every 1000 steps (corresponding to a time interval of 4 ps), and had an initial height of 0.1 kcal mol^{-1} and a sigma value of 0.2 nm (CV1) and 7.5° (CV2). The width of the Gaussian functions determines the resolution of the reconstructed free energy profile. To assess convergence of the metadynamics simulations we assessed the proper sampling of both CVs and we calculated the free energy profile as a function of time (every 5 ns). We observed that, after 200 ns, the estimates did no longer change over time.

Binding free energy calculations

To compute the Amadoriase I-FLY standard (absolute) binding free energy, alchemical free energy perturbation (FEP) molecular dynamics calculations were performed in which the ligand was decoupled from its binding site within the protein, as well as from bulk water. The total free energy of binding is expressed as the reversible thermodynamic work needed for sequentially switching on the interaction of the ligand with its surrounding (receptor and solvent) (Fig. 2). The starting coordinates for decoupling of the ligand from the bound state in the

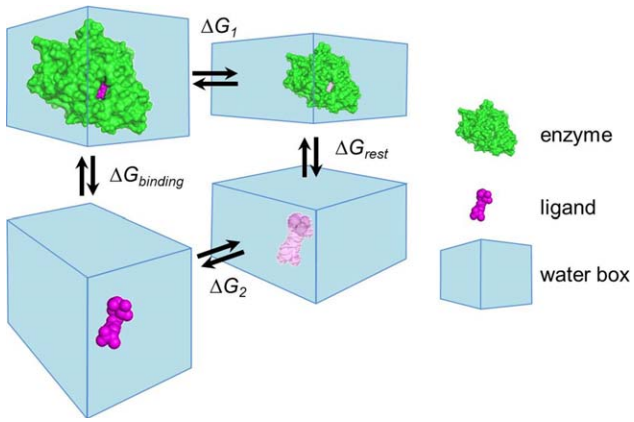

Figure 2

Thermodynamic cycle used to calculate the reversible association of FLY to Amadoriase I. [Color figure can be viewed in the online issue, which is available at wileyonlinelibrary.com.]

Amadoriase I binding site were taken from the corresponding MD simulations of the complex after 1 μs. For the simulation of FLY decoupling from plain water, the ligand was solvated in a water box of the same size as the protein box. The Amber ff99SB force field[34] was used for all the simulations performed with the NAMD2.9 software[36]. The binding free energy of the ligand was calculated using the "double decoupling method".[44] The coupling λ parameter was smoothly varied between 1 (corresponding to a full electrostatics and van der Waals interactions) and 0 (where no electrostatics or van der Waals interaction with the force field are considered) in steps of 0.02 using 50 windows. Forward and backward runs were performed in NVT ensemble with 2 fs as time step at reference temperature of 310K. We used 20 ps equilibration runs followed by 40 ps of production runs for each window, which were then combined using the Simple Overlap Sampling Method[45] since the overlap of forward and backward runs provides information on the convergence of the process, showing microreversibility of the transformation. In the simulation protocol, in order to control orientational and translational movements of FLY relative to the binding site for λ approaching 0, restraining harmonic potentials with a constant $k = 5$ kcal mol^{-1} $Å^{-2}$ or $k = 5$ kcal mol^{-1} rad^{-2} were activated using the Colvars module of NAMD. We imposed translational and rotational restrictions on the distances between FLY and the nearby residues (Trp240, Gly370, Asn371) as well as between FLY and the enzyme cofactor, on the sugar moiety orientation relative to the amino acid part through a dihedral angle and on the terminal part of the lysine moiety through an angle COLVAR component. We also included H-bond COLVAR components between FLY and receptor residues that form stabilizing interactions in the crystal structure (Arg418, Glu285, Glu59, Gly371, and Asn372).

The effect of this restrain potential was removed at the end of the FEP calculations. Theoretically, the total standard binding free energy is not affected by restraints.[46,47] The total free energy change is expressed as:[48,49]

$$\Delta G_{\text{binding}} = (\Delta G_2 - \Delta G_1) + \Delta G_{\text{rest}} = (\Delta G_{\text{annihil, bulk}} - \Delta G_{\text{annihil, bound}}) + \Delta G_{\text{rest}} \quad (1)$$

$$\Delta G_{\text{rest}} = (\Delta G_{\text{C, bulk}} - \Delta G_{\text{C, bound}}) + \Delta G_{\text{r}} + \Delta G_{\text{t}} \quad (2)$$

where $\Delta G_{\text{annihil, bulk}} - \Delta G_{\text{annihil, bound}}$ corresponds to the interaction free energy difference associated with removing the ligand from the bulk solution and inserting it in the binding site, ΔG_{rest} corresponds to the free energy cost arising from the conformational (c), translational (t), and rotational (r) freedom restriction of the ligand upon binding.[46] The use of these restrictions allows for thermodynamic microreversibility as it accounts for the loss of entropy that is associated with ligand binding to the receptor, where the ligand is expected to be more restricted than it is in bulk solvent. This allows faster convergence and circumvents the "wandering-ligand" issue.[48,50–52]

Enzymatic activity

Amadoriase I activity was assessed by measuring the rate of formation of glucosone from fructosyl-lysine using a colorimetric reaction with o-phenylenediamine (OPD) and monitoring absorbance at 322 nm, as described in previous works.[10,11] The reaction was carried out in a solution containing 10 m*M* sodium phosphate buffer pH 7.4, FLY 20 m*M*, OPD 50 m*M*. The enzyme was added at 60 n*M* from batches stocked at different temperatures (+4°C, −20°C and −80°C) in a final volume of 1 mL and incubated for up to three hours at 37°C.

We also tested the ability of Amadoriase I to prevent the formation of pentosidine crosslink between lysine and arginine in the presence of reducing sugars.[5,53] The glycation of lysine, with arginine, in the presence of Amadoriase I was carried out in 10 m*M* sodium phosphate buffer, pH 7.4, using the following conditions: lysine 50 m*M*, arginine 50 m*M*, ribose 100 m*M*, Amadoriase I 600 n*M*, or 60 n*M* in a final buffer volume of 500 mL. The mixture was incubated at 37°C for up to 5 days, while the glycation reaction was monitored by measuring the absorbance at 365 nm.[54,55] Ribose was chosen as glycating agent owing to its higher reactivity compared to glucose.[54]

RESULTS AND DISCUSSION

Amadoriase enzymes belong to the FAD-binding protein family of oxidoreductases. Their two-domain architecture comprises a classic FAD-binding motif formed by four α-helices packed against two β-sheets, and a catalytic domain formed by an 8-stranded mixed β-sheet and two long α-helices, one of which is located on top of the active site. To date, the only known structures available of this family are the structure of Amadoriase II,[24] both in its free form (PDB code: 3DJD) and in complex with the inhibitor fructosyl-thyoacetate (FSA) (PDB code: 3DJE), and the structure of FPOX-E in free form (PDB code: 4RSL).[25] However, the Amadoriase II in free form could only be partially traced in the electron density map, thus affording an incomplete structural model that did not allow some of the most crucial mechanistic details of the enzyme to be clarified. In particular, the structure entirely lacks two crucial loops that, given their proximity to the catalytic site, may either contribute to defining its size or allow substrate accessibility to the active site or be dynamically involved in substrate recognition and binding. On the other hand, FPOX-E has only been determined in its apo form and is not available in its ligand-bound configuration. Understandably, this only partial structural characterization of Amadoriases has so far negatively impacted on the rational engineering approach to the development of effective enzymatic tools for protein deglycation.

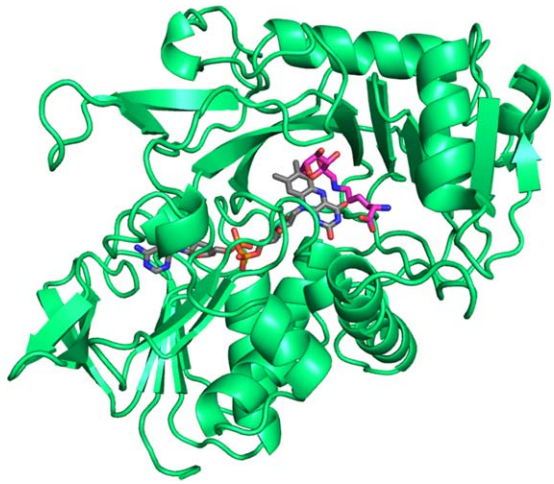

Figure 3

Crystal structure of Amadoriase I in complex with fructosyl-lysine. The protein (green) is shown as a cartoon model while FLY (purple) and FAD (grey) are shown as stick models.

In this work, we report the complete crystal structure determination of Amadoriase I from *Aspergillus fumigatus* in its free form (determined at 1.6 Å resolution) and in complex with its natural substrate N^{ϵ}-fructosyl-lysine (FLY) (determined at 1.9 Å resolution) (Fig. 3). In both cases, two independent molecules are present in the asymmetric unit. In both crystals, the two independent molecules are nearly identical as their main chain atoms

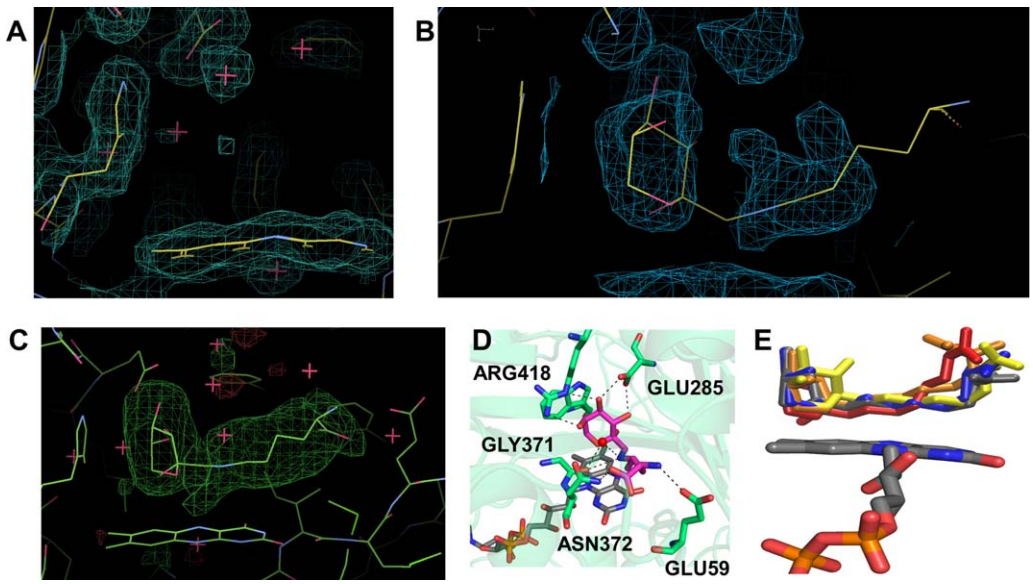

Figure 4

Structure of the Amadoriase I catalytic pocket. Comparison of the 2Fo-Fc map in the active site of the enzyme in the apo (**A**) and in the substrate-bound (**B**) structures. Both maps are contoured at the 0.8 σ-level. **C**: Superposition of the FLY structure on the Fo-Fc OMIT map of the active site, contoured at the 3 σ-level. **D**: Interactions of the catalytic residues with FLY in the ligand-bound crystal structure of Amadoriase I. **E**: FLY configuration clusters observed during MD calculations. [Color figure can be viewed in the online issue, which is available at wileyonline library.com.]

superimpose with an r.m.s.d. of 0.223 Å and 0.230 Å, respectively. Moreover, when the free and the substrate-bound Amadoriase I structures are superimposed, an r.m.s.d. of 0.243 Å for main chain atoms can be calculated, suggesting that, globally, only small conformational changes are induced in the overall structure upon ligand binding.

The electron density map of the Amadoriase I-substrate complex showed clear electron density in the active site [Fig. 4(A–C)]. However, although this electron density could be identified as the FLY substrate, the best model and refinement statistics were obtained by assigning FLY a 0.7 occupancy factor in the crystal. Co-crystallization of Amadoriase I and its natural substrate FLY was obtained by incubating the protein sample with a 300-fold molar excess of FLY in a nitrogen atmosphere inside a glove box. The sample was subsequently mixed with the crystallization buffer using the hanging drop vapor diffusion method, as described in the material and methods section. All steps of the co-crystallization procedure were carried out in an oxygen-free atmosphere in order to inhibit or limit enzyme activity. It is conceivable that the partial ligand occupancy may reflect substrate turnover resulting from the presence of residual oxygen during the crystallization and crystal manipulation steps.

In the active site of the enzyme, FLY forms a stabilizing network of hydrogen bonds, as shown in Figure 4(D). The sugar unit is stabilized by two hydrogen bonds with the side-chain of Arg418 (2.92 and 3.01 Å), and two hydrogen bonds with the side-chain of Glu285 (2.69 and 2.76 Å). The lysine moiety of the FLY ligand forms a hydrogen bond between its NH_3^+ group and the carbonyl oxygen of Glu59 (2.99 Å), a second hydrogen bond between one of the oxygen atoms of its carboxy group and the amide nitrogen of Asn372 (2.73 Å) and a third hydrogen bond between the N^{ϵ} atom of lysine and the carbonyl oxygen of Gly371 (3.13 Å). The importance of these contacts is confirmed by mutagenesis experiments that are available in the literature. The work of Collard and co-workers[24] on Amadoriase II showed that the mutation of either Glu285 or Arg418 (that is, their homologous in Amadoriase I) leads to a totally inactive enzyme. A further clear evidence of the importance of these two residues is that they are invariably conserved in all Amadoriases (Fig. 5). Similarly, Miura and co-workers showed that the mutation of the conserved Gly371 residue (i.e, its homologous in N1-1 FAOD) leads to an inactive enzyme.[65] Conversely, Glu59 and Asn372 residues are not conserved among the different Amadoriases (Fig. 5) and have been shown to tune the selectivity of the enzymes toward different glycated amino acids. Miura and co-workers[59,63] performed mutagenesis experiments on N1-1 FAOD in these two positions, showing that the double mutant His51Lys/Asn354His has greater selectivity for f-Val then for f-Lys, a favorable feature for the detection of glycated hemoglobin.

Further complex stabilization is provided by the FLY second carboxy oxygen, which makes a water mediated

contact with the carbonyl oxygen of Glu59. Lysine N_ϵ forms both a direct hydrogen bond with the carbonyl oxygen of Gly371, and a water-mediated hydrogen bond with the same residue [Fig. 4(D)]. This water molecule forms an extensive network of hydrogen bonds with the surrounding residues and is not present in the free structure; this is suggestive of a catalytic role for this water molecule in the hydrolysis of the substrate. Complex stabilization energy is provided also by van der Waals contacts between the sugar ring and both the side-chain of Trp241 and FAD. Moreover, the alkyl chain of FLY forms several hydrophobic contacts with the surrounding residues (Ile57, Met375, Phe101 and Phe263) and with FAD, despite showing slightly different conformations in the two substrate-bound Amadoriase I monomers that are present in the asymmetric unit. The lysine moiety of the ligand is in fact rather flexible. This is highlighted by the observed high B-factors of the lysine tail in the crystal structure. The ligand flexibility is also confirmed by the microsecond-long molecular dynamics simulation (see MD trajectory in the Supplementary Informations). The trajectory analysis confirms the multiple direct hydrogen bonds between the protein and the ligand, where the most persistent bonds are those involving two hydroxyl groups of the sugar ring, which form hydrogen bonding interactions with Glu285 for 50.8% and 70.9% of the 1 μs time-course simulation, respectively. Further stabilizing hydrogen bonds are formed between the third hydroxyl group of the sugar ring and Arg418 (17.0%), the lysine N^ϵ and Gly371 (14.4%), the FLY NH_3^+ group and Glu59 (30.0%) and the FLY COO^- group and Asn371 (7.9%). The strong interaction of the sugar ring with the protein and, conversely, the high flexibility of the FLY tail are confirmed by the analysis of the FLY conformation during the MD run. The clustering of the 10'000 frames obtained during the MD simulation results in five different conformational clusters, which differ almost exclusively for the configuration of the FLY tail [Fig. 4(E)].

While in the free form of Amadoriase I the Asn372 residue is disordered, its conformation is stabilized upon binding to the carboxy terminal of FLY in the substrate-bound Amadoriase I structure, suggesting a substrate recognition role for this residue.

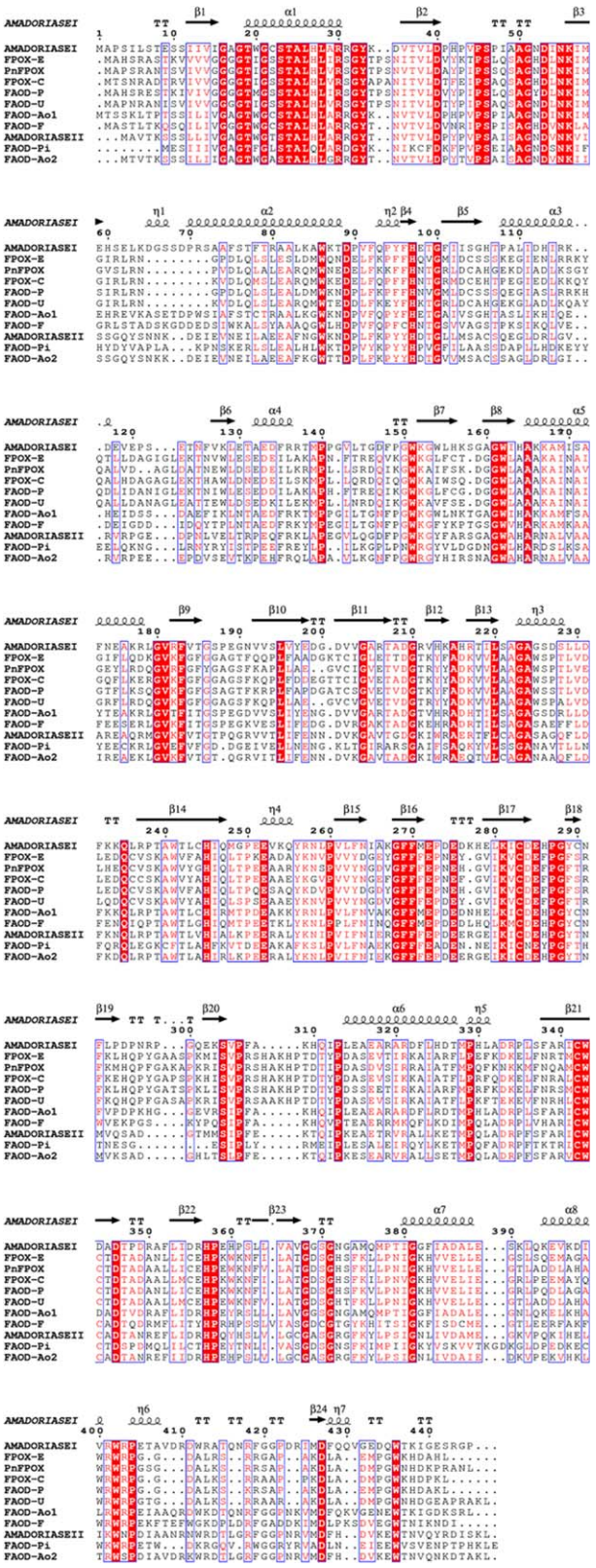

Figure 5

Structure-based sequence alignment of *Aspergillus fumigatus* Amadoriase I with the other known FAOX enzymes. The secondary structure of Amadoriase I enzyme is presented in the first line. Residues are coloured based on their conservation: red box with white characters means strict identity, red characters indicate similarity among residues involved. The alignment is performed with Clustal Omega software[56] and presented using Esprit 3.0 software[57]. The sequences used for the alignment are: FPOX-E from *E.terrenu*m ATCC 18547[58], PnFPOX from *Phaeosphaeria nodorum* SN15[59], FPOX-C from *Coniochaeta sp* NISL 9330[60], FAOD-P from *Penicillum janthinelum* AKU 3413[61], FAOD-U from *Ulocladium sp.* JS-103[62], FAOD-Pi from *Pinchia sp.* N1-1[63], FAOD-Ao1 and FAOD-Ao2 from *A. oryzae*[61], Amadoriase II and Amadoriase I from *A. fumigatus*[21], FAOD_F form *Fusarium oxysporum*[64]. [Color figure can be viewed in the online issue, which is available at wileyonlinelibrary.com.]

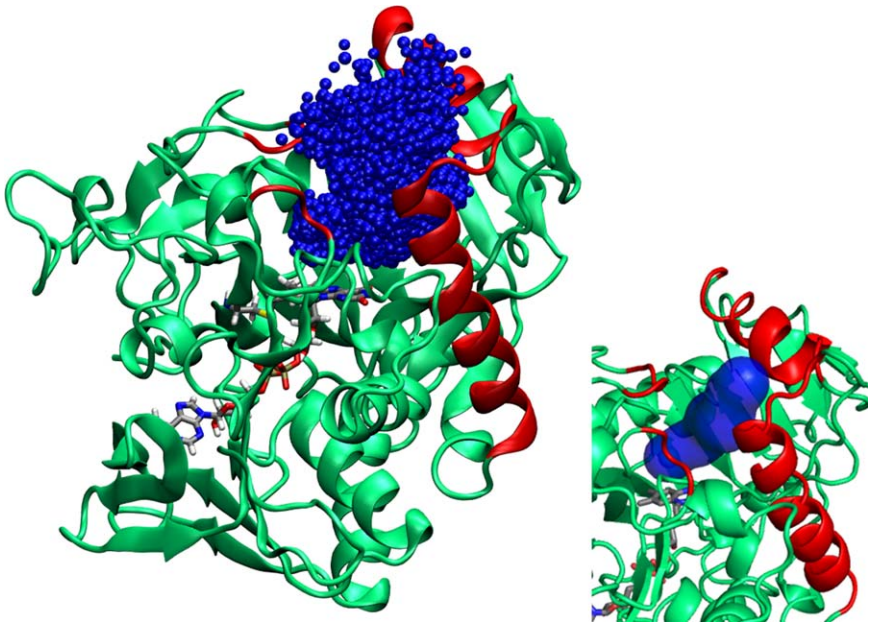

Figure 6

V**olume explored during RAMD simulations (shown in blue)**. In the inset, tunnel conformation calculated by CAVER. The sections shown in red highlight the gating loop and helices. [Color figure can be viewed in the online issue, which is available at wileyonlinelibrary.com.]

Tunnel conformation, egress trajectory, and free energy profile

The tunnels connecting the active site of Amadoriase I with bulk solvent were analysed with the CAVER 3.0.1 plugin[40] of PyMol.[44] The results show that there is a single possible tunnel for ligand entry, featuring a bottleneck of ≈2.8 Å and a distance of ≈18 Å from FAD surface to bulk water. The exit of the tunnel is defined by two loops (residues 349–351 and 416–420) and two alpha-helices (residues 108–121 and 67–88) (Fig. 6). These results are confirmed by the egress trajectory, as calculated from RAMD simulations. In all different trials, starting from different frames extracted from the equilibration run, the ligand leaves the binding pocket from the tunnel identified by CAVER. Furthermore, the RAMD trajectory allows for the identification of the internal available volume, which is rather large, roughly "L-shaped" and is connected to the bulk solvent by a much narrower tunnel.

The energetics of the Amadoriase I tunnel from bulk water to the binding cavity was explored using metadynamics simulations,[42,43] in which the molecular dynamics run is biased by a history-dependent potential defined as the sum of Gaussian functions in the CV space. In our study, we monitored the free energy as a function of the distance and orientation between the FLY ligand and FAD [Fig. 7(A)]. The free energy surface shows that the free energy minimum corresponds to the crystallographic position, where the FLY-FAD distance is ≈3.5 Å and the angle between FLY and FAD is ≈60° [Fig. 7(B)]. The ligand's approach to the cavity occurs through a narrow passage (corresponding to FLY-FAD distances in the 4 to 10 Å range) in which the FLY orientation is restrained, assuming angle values linearly decreasing from 150° to 60° while approaching the catalytic position. For FLY-FAD distances between 10 and 14 Å, the enzyme presents a larger cavity in which reorientation of the ligand is possible without a steep increase in the energy. The gate to the tunnel entrance is positioned at a FLY-FAD range distance of 16–18 Å. The entrance of the ligand is possible in two different orientations. In the "head first" conformation, the ligand enters with the sugar ring first, assuming an angle of 111° with respect to FAD. On the other hand, in the "tail first" conformation, the lysine chain enters the tunnel before the ring, thus assuming an angle of 50° with respect to FAD. In this latter case, the reorientation of the ligand occurs within the larger inner cavity, before reaching the narrow tunnel leading to the catalytic site. These results confirm the role of the gating loops in restraining access to the tunnel.

The total binding free energy of Amadoriase I with its natural substrate, FLY, was evaluated using alchemical free energy simulations. Our results showed a total binding free energy of -8.4 ± 2.0 kcal/mol with an average net free energy during annihilation transformation for free and bound ligand of -24.8 kcal/mol and -2.28 kcal/mol respectively, and a total restrain potentials

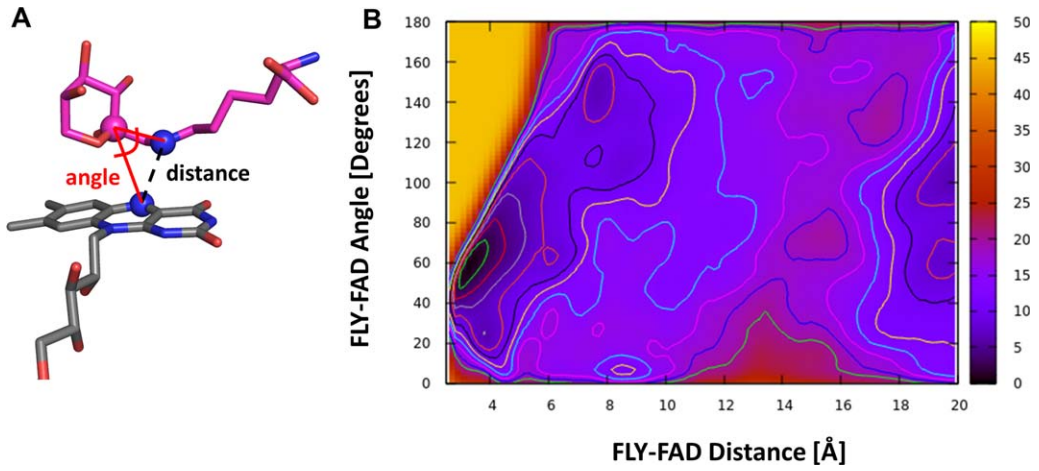

Figure 7

Metadynamics simulations. A: The collective variables chosen for metadynamics simulations. The first CV (FLY-FAD distance) is the distance between the FLY N^{ϵ} atom and the FAD N(5) atom, whereas the second CV (FLY-FAD angle) is defined as the angle between the lysine N^{ϵ} atom, the sugar ring C(1) atom and the FAD N(5) atom. **B**: Free energy surface as a function of the two collective variables. The free energy minimum, corresponding to the catalytic position, is found for a FAD-FLY distance of ≈3.5 Å and for an angle between FLY and FAD of ≈60°. The entrance of the tunnel is located at a distance of ≈18 Å. [Color figure can be viewed in the online issue, which is available at wileyonlinelibrary.com.]

contribution of 14.1 kcal/mol. This estimation is in good agreement with metadynamics results, where the global energetic minimum is ≈ −8 kcal/mol with respect to bulk water.

Enzymatic assays

A complete characterization of the Amadoriase I kinetic parameters and binding affinity for different substrates has been already described in previous works.[10,21,24,66–68] Here, we provide evidence of catalytic activity of the purified enzyme used for structure determination. The enzymatic activity of Amadoriase I was measured by recording the amount of glucosone released from the fructosyl-lysine in the course of the deglycation reaction [Fig. 8(A)]. Figure 8(B) reports glucosone release in the presence of Amadoriase I showing a significant increase in absorbance at 365 nm during the 60-min monitoring time, proving that the deglycating enzyme is active. Moreover, the data show that storage conditions (4, −20 and −80°C) do not influence significantly the enzyme activity toward the glycated substrate.

We tested the ability of Amadoriase I to prevent the formation of stable cross-linking AGEs (pentosidine) between lysine and arginine. The results [Fig. 8(C)] show that the presence of ribose induces a marked increase in absorbance, which is associated with the increase of general AGEs, the pentosidine crosslink in particular. Conversely, the presence of Amadoriase I strongly reduces the formation of glycation products, since there is no significant difference in the absorbance levels between the control samples and the samples including the reducing sugar and Amadoriase I.

Comparison of Amadoriase I and other FAOX enzymes

A sequence alignment of Amadoriase I and the other known FAOX enzymes is shown in Figure 5, displaying a high level of identity and homology among the different members of this family. A structure superposition of Amadoriase I with the available structures of Amadoriase II (free and bound form) and FPOX-E (free form) is shown in Figure 9(A). Globally, despite the fact that the three enzymes belong to different groups of FAOX, their overall folding architecture is highly conserved. The major differences between them reside in the conformation of the loops (residues 59–70 and 121–126) that are close to the amino acid moiety of the ligand [Fig. 9(B,D)].

In the FAD-binding domain of Amadoriase I, the cofactor is in the same extended conformation found in both the free and the inhibitor-bound structures of Amadoriase II as well as in the free structure of FPOX-E, forming stabilizing interactions with a number of conserved residues. FAD is bound to almost the same residues in Amadoriase I and Amadoriase II or FPOX-E, and its conformation and orientation are maintained in all available crystal structures. Residues Thr19, Trp20, Asp40, Ala50, Val192, and Gly373 in Amadoriase I are all involved in FAD binding, as are their conserved counterparts in Amadoriase II (Thr16, Trp17, Asp37, Ala47, Val187 and Gly366, respectively) and their partly conserved homologues in FPOX-E. Interestingly, Gly373, like its Amadoriase II conserved counterpart Gly366, makes both an H-bonding interaction with a FAD hydroxyl group and an H-bond with the N atom of the Trp20 side-chain through its carbonyl group. This highlights

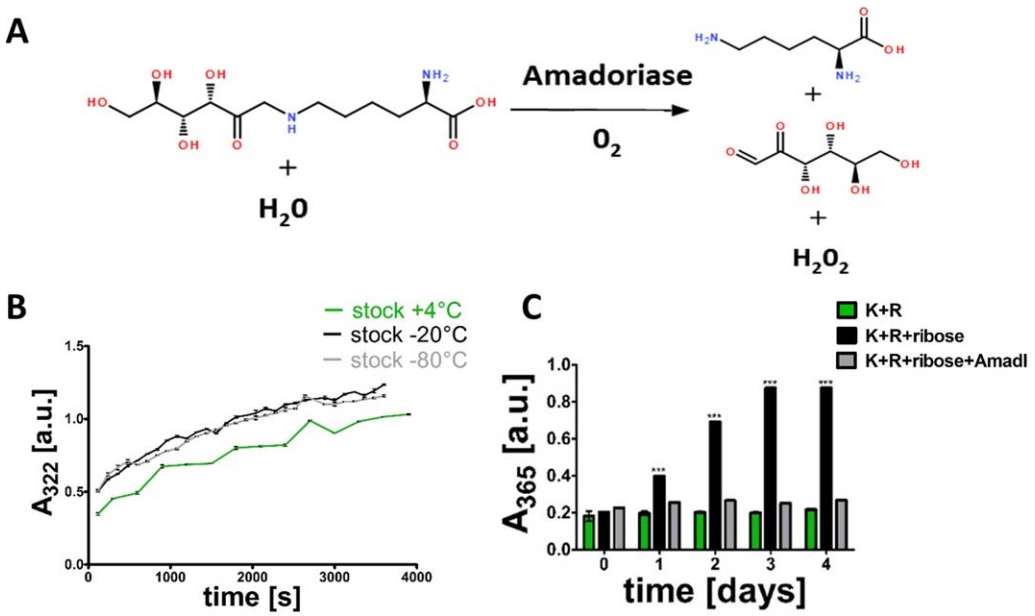

Figure 8

Enzymatic assays. A: Schematic of the reaction catalyzed by Amadoriase I: the oxidation of fructosysl-lysine produces a free amine, glucosone and hydrogen peroxide. **B**: Enzyme activity was evaluated over time with a colorimetric reaction measuring glucosone release as product of the enzymatic reaction of Amadoriase I with its natural substrate fructosyl-lysine. Glucosone formation was monitored by OPD assay at 322 nm. The rate of glucosone production is independent from the stocking temperature of the enzyme. **C**: Enzyme glycation prevention ability is measured in terms of ribose-mediated glycation of lysine and arginine in the presence/absence of Amadoriase I by monitoring absorbance at 365 nm. The presence of Amadoriase I clearly results in a negligible glycation rate, as shown by the comparable absorbance levels and by the lack of absorbance increase over time relative to the controls (pure amino acids). A significant difference (*** $p < 0.01$, Kruskal Wallis test with 15 repetitions for sample) can be observed between glycation in the absence (black) and in the presence (grey) of Amadoriase I. [Color figure can be viewed in the online issue, which is available at wileyonlinelibrary.com.]

the important structural role played by the conserved Gly373 residue.

Unlike the free form of Amadoriase II, the entire electron density map of the apo-Amadoriase I structure reported herein could be completely and unambiguously assigned in all its parts, including the two long loop portions [residues 59–70 and 121–126, respectively, Fig. 9(B,D)] near the active site that are not visible in the apo-Amadoriase II structure and that provide close stabilizing contacts with FSA in the inhibited form of Amadoriase II [Fig. 9(A)]. By comparison with the FSA-inhibited form of Amadoriase II and the free form of FPOX-E, the conformation of the 59–70 loop of Amadoriase I helps to form a much larger active site than in the other two Amadoriases by extending itself toward the bulk water rather than toward the core [Fig. 9(B)], thus allowing for the insertion of a bulkier substrate. In fact, in both the free and the substrate-bound forms of Amadoriase I, residues His60 within the loop and Thr79 within the adjacent alpha helix form a stabilizing hydrogen bonding interaction that holds the loop in its observed conformation, projected away from the catalytic site, while in the FSA-bound Amadoriase II structure the corresponding amino acids, Ser57 and Ala74, do not form any contacts with each other, thus leaving the two loops free to fold toward the active site upon substrate binding and contribute to ligand stabilization. Likewise, in Amadoriase I, an hydrogen bond between Glu62 and Glu123 and one between Lys64 and Glu120 also help to keep the two loops in the observed relative conformation. In the inhibited form of Amadoriase II, the lack of stabilizing hydrogen bonds between the two loops, which could not be determined in the apo form, suggest a high degree of flexibility in these two portions of the protein. In other words, the 59–70 loop in Amadoriase I maintain the same conformation in the free and in the substrate-bound structures and, unlike the corresponding loops in Amadoriase II, it does not fold inwards to help stabilize the substrate in the active site. The tight regulation of the conformation of this loop appears to be a structural determinant of the size of the catalytic site. Interestingly, at the end of the 59–70 loop in Amadoriase I residue Pro70 makes the following α-helix one turn shorter than in Amadoriase II, in which the corresponding residue is an isoleucine. Similarly, Pro121 at the end of the 121–126 loop shortens the following α-helix with respect to the same secondary structure element of Amadoriase II.

The three residues in Amadoriase II that are known to bind the sugar moiety of the substrate (Glu280, Gly364,

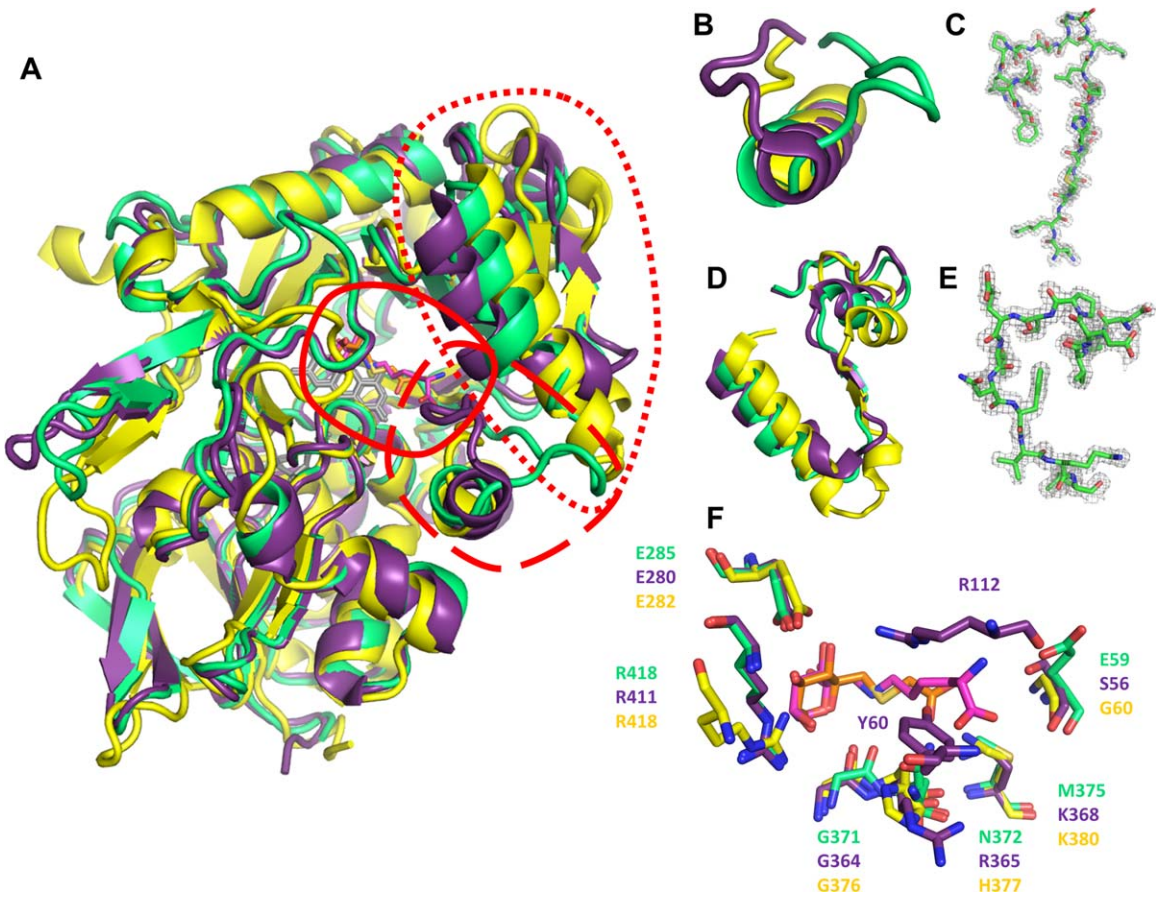

Figure 9

Structural comparison of Amadoriase I (green), Amadoriase II (purple), and FPOX-E (yellow). A: Superimposition of the ligand-bound crystal structures of Amadoriase I, Amadoriase II, and FPOX-E. The dashed red circle highlights the different arrangement of loop 59–70 (Amadoriase I numbering), detailed in panel **B**. While in Amadoriase II and FPOX-E this loop is directed toward the core of the protein, in Amadoriase I the loop is projected outward and is exposed to the solvent, thus contributing to the formation of a larger catalytic cavity. The dotted red circle highlights the different arrangement of loops 121–126 (Amadoriase I numbering) and surrounding regions, detailed in panel D. Panel (**C–E**) show the clear and well-defined electron density map for the two loops in the Amadoriase I structures reported here. (**F**) Superimposition of Amadoriase I (green), Amadoriase II (purple) and FPOX-E active site (full red line in panel A), showing the side chains of residues surrounding the ligand/inhibitor (FLY in pink, FSA in orange). [Color figure can be viewed in the online issue, which is available at wileyonlinelibrary.com.]

Arg411) are completely conserved in all Amadoriases (Fig. 5) and they assume a very similar conformation in all available structures [Fig. 9(F)], suggesting that the catalytic mechanism is similar across this class of enzymes. The major difference between the three structures is the size of the active site, which is related to the different conformation of the 59–70 loop, and the residues binding the amino acid moiety of the ligand, which affect the specificity of each FAOX. A number of residues that are found in the vicinity of the active site are likely to be involved in substrate recognition. Residue Ile57 in Amadoriase I corresponds to Val54 in Amadoriase II. It is possible that the slightly longer side-chain facilitates hydrophobic contacts with the long side-chain of the fructosyl-lysine when the substrate is bound to the active site in the same orientation as the fructosyl-glycine substrate in Amadoriase II, thus holding it straight. Residue Met375 in Amadoriase I replaces residue Lys368 in Amadoriase II. While in Amadoriase II Lys368 forms an hydrogen bond between its side-chain amino group and the carboxy group of FSA, in Amadoriase I Met375 contributes to the stabilization of the long side-chain of the substrate by means of hydrophobic contacts.

Interestingly, in the structure of Amadoriase II, Tyr60 belongs to the loop whose structure could be only determined in the inhibited form of the enzyme, where the loop is folded toward the active site and coordinates the FSA inhibitor. In that structure, Tyr60 binds directly the substrate and it also forms an hydrogen bond with a water molecule that contacts the sulphur atom of the FSA inhibitor. Conversely, in Amadoriase I there is clearly no contribution to the stabilization and processing of the substrate from residues in the loops. However a water molecule is observed in the same position also in

Amadoriase I, albeit stabilized by Gly371 [Fig. 4(D)]. Hence, the comparison between the ligand-bound forms of Amadoriase I and Amadoriase II suggests a catalytic role for this water molecule.

CONCLUSIONS

In conclusion, the high resolution crystal structures of the free and the substrate-bound forms of Amadoriase I shown here allow for a clear identification of the substrate recognition residues of the enzyme and provide a complete description of the architecture of its active site, including the crucial loops that remained elusive in the crystal structure of the free form of the related Amadoriase II enzyme. Comparison with the previously determined crystal structure of the FSA-inhibited form of Amadoriase II allows for the elucidation of the substrate recognition process in these two homologous enzymes and the molecular bases of their specificity. This paves the way to future enzyme engineering studies aimed at developing protein deglycation tools that can positively reverse cellular aging processes as well as diabetes-related alterations in all human tissues. In fact, by means of a combined mutagenesis and structure assessment approach, an engineered Amadoriase-like enzyme that can efficiently recognize and process larger substrates such as glycosylated amino acids within proteins can likely be designed and utilized therapeutically to prevent or reverse AGEs accumulation in aging tissues. Moreover, precise structural date can favor the development of novel Amadoriases with enhances selectivity for f-Val, to be used as diagnostic tools for monitoring diabetes.

ACCESSION NUMBERS

The final crystallographic coordinates of the two structures are available in the RCSB PDB (accession code: 4WCT and 4XWZ).

ACKNOWLEDGEMENTS

The authors wish to thank the X06DA-PXIII beamline personnel of the Paul Scherrer Institute, Villigen Switzerland, for help with the data collection. High-performance computing resources have been provided by CINECA Consortium through the ISCRA initiative. The authors thank Prof. Gabriele Candiani for providing laboratory equipment for the enzymatic assays, Dr. Simona M. Monti, Dr. Giovanni Roviello and Prof. Vincenzo Fogliano for kindly providing the enzyme substrate, and Dr. Marco Piola for the use of the glove box.

REFERENCES

1. Bailey AJ. Molecular mechanisms of ageing in connective tissues. Mech Ageing Dev 2001;122:735–755.
2. Avery NC, Bailey AJ. The effects of the Maillard reaction on the physical properties and cell interactions of collagen. Pathol Biol 2006;54:387–395.
3. Goh SY, Cooper ME. The role of advanced glycation end products in progression and complications of diabetes. J Clin Endocr Metab 2008;93:1143–1152.
4. Sell DR, Monnier VM. Molecular basis of arterial stiffening: Role of glycation—A mini-review. Gerontology 2012;58:227–237.
5. Grandhee SK, Monnier VM. Mechanism of formation of the maillard protein cross-link pentosidine—Glucose, fructose, and ascorbate as pentosidine precursors. J Biol Chem 1991;266:11649–11653.
6. John WG. Haemoglobin A1c: Analysis and standardisation. Clin Chem Lab Med 2003;41:1199–1212.
7. Monnier VM, Wu X. Enzymatic deglycation with amadoriase enzymes from Aspergillus sp. as a potential strategy against the complications of diabetes and aging. Biochem Soc Trans 2003;31: 1349–1353.
8. Wu X, Monnier VM. Enzymatic deglycation of proteins. Arch Biochem Biophys 2003;419:16–24.
9. Monnier VM, Mustata GT, Biemel KL, Reihl O, Lederer MO, Dai ZY, Sell DR. Cross-linking of the extracellular matrix by the Maillard reaction in aging and diabetes—An update on "a puzzle nearing resolution". Ann NY Acad Sci 2005;1043:533–544.
10. Mennella C, Borrelli RC, Vinale F, Ruocco M, Fogliano V. Substrate specificity of amadoriase I from Aspergillus fumigatus. Ann NY Acad Sci 2005;1043:837–844.
11. Capuano E, Fedele F, Mennella C, Visciano M, Napolitano A, Lanzuise S, Ruocco M, Lorito M, Del Castillo MD, Fogliano V. Studies on the effect of amadoriase from Aspergillus fumigatus on peptide and protein glycation in vitro. J Agr Food Chem 2007;55: 4189–4195.
12. Lin ZL, Zheng J. Occurrence, characteristics, and applications of fructosyl amine oxidases (amadoriases). Appl Microbiol Biot 2010; 86:1613–1619.
13. Reigle KL, Di Lullo G, Turner KR, Last JA, Chervoneva I, Birk DE, Funderburgh JL, Elrod E, Germann MW, Surber C, Sanderson RD, Antonio JDS. Non-enzymatic glycation of type I collagen diminishes collagen-proteoglycan binding and weakens cell adhesion. J Cell Biochem 2008;104:1684–1698.
14. Gautieri A, Redaelli A, Buehler MJ, Vesentini S. Age- and diabetes-related nonenzymatic crosslinks in collagen fibrils: Candidate amino acids involved in advanced glycation end-products. Matrix Biol 2014;34:89–95.
15. Verzijl N, DeGroot J, Ben Zaken C, Braun-Benjamin O, Maroudas A, Bank RA, Mizrahi J, Schalkwijk CG, Thorpe SR, Baynes JW, Bijlsma JWJ, Lafeber FPJG, TeKoppele JM. Crosslinking by advanced glycation end products increases the stiffness of the collagen network in human articular cartilage—A possible mechanism through which age is a risk factor for osteoarthritis. Arthritis Rheum 2002; 46:114–123.
16. Svensson RB, Mulder H, Kovanen V, Magnusson SP. Fracture mechanics of collagen fibrils: Influence of natural cross-links. Biophys J 2013;104:2476–2484.
17. Tang SY, Vashishth D. The relative contributions of non-enzymatic glycation and cortical porosity on the fracture toughness of aging bone. J Biomech 2011;44:330–336.
18. Semba RD, Nicklett EJ, Ferrucci L. Does accumulation of advanced glycation end products contribute to the aging phenotype? J Gerontol A Biol 2010;65:963–975.
19. Troise AD, Dathan NA, Fiore A, Roviello G, Di Fiore A, Caira S, Cuollo M, De Simone G, Fogliano V, Monti SM. Faox enzymes inhibited Maillard reaction development during storage both in protein glucose model system and low lactose UHT milk. Amino Acids 2014;46:279–288.
20. Deppe VM, Bongaerts J, O'Connell T, Maurer KH, Meinhardt F. Enzymatic deglycation of Amadori products in bacteria:

Mechanisms, occurrence and physiological functions. Appl Microbiol Biot 2011;90:399–406.
21. Takahashi M, Pischetsrieder M, Monnier VM. Isolation, purification, and characterization of amadoriase isoenzymes (fructosyl amine-oxygen oxidoreductase EC 1.5.3) from Aspergillus sp. J Biol Chem 1997;272:3437–3443.
22. Zheng J, Guan H, Xu LH, Yang R, Lin ZL. Engineered amadoriase II exhibiting expanded substrate range. Appl Microbiol Biot 2010; 86:607–613.
23. Qian Y, Zheng J, Lin ZL. Loop engineering of amadoriase II and mutational cooperativity. Appl Microbiol Biot 2013;97:8599–8607.
24. Collard F, Zhang J, Nemet I, Qanungo KR, Monnier VM, Yee VC. Crystal structure of the deglycating enzyme fructosamine oxidase (amadoriase II). J Biol Chem 2008;283:27007–27016.
25. Gan W, Gao F, Xing K, Jia M, Liu H, Gong W. Structural basis of the substrate specificity of the FPOD/FAOD family revealed by fructosyl peptide oxidase from Eupenicillium terrenum. Acta Crystallogr F Struct Biol Commun 2015;71:381–387.
26. Ferri S, Kim S, Tsugawa W, Sode K. Review of fructosyl amino acid oxidase engineering research: A glimpse into the future of hemoglobin A1c biosensing. J Diabetes Sci Technol 2009;3:585–592.
27. Troise AD, Fiore A, Roviello G, Monti SM, Fogliano V. Simultaneous quantification of amino acids and Amadori products in foods through ion-pairing liquid chromatography-high-resolution mass spectrometry. Amino Acids 2015;47:111–124.
28. Vinale F, Fogliano V, Schieberle P, Hofmann T. Development of a stable isotope dilution assay for an accurate quantification of protein-bound N-epsilon-(1-deoxy-d-fructos-1-yl)-l-lysine using a C-13-labeled internal standard. J Agr Food Chem 1999;47:5084–5092.
29. Vagin A, Teplyakov A. Molecular replacement with MOLREP. Acta Crystallogr D 2010;66:22–25.
30. Winn MD, Ballard CC, Cowtan KD, Dodson EJ, Emsley P, Evans PR, Keegan RM, Krissinel EB, Leslie AGW, McCoy A, McNicholas SJ, Murshudov GN, Pannu NS, Potterton EA, Powell HR, Read RJ, Vagin A, Wilson KS. Overview of the CCP4 suite and current developments. Acta Crystallogr D 2011;67:235–242.
31. Murshudov GN, Skubak P, Lebedev AA, Pannu NS, Steiner RA, Nicholls RA, Winn MD, Long F, Vagin AA. REFMAC5 for the refinement of macromolecular crystal structures. Acta Crystallogr D 2011;67:355–367.
32. Adams PD, Afonine PV, Bunkoczi G, Chen VB, Davis IW, Echols N, Headd JJ, Hung LW, Kapral GJ, Grosse-Kunstleve RW, McCoy AJ, Moriarty NW, Oeffner R, Read RJ, Richardson DC, Richardson JS, Terwilliger TC, Zwart PH. PHENIX: A comprehensive Python-based system for macromolecular structure solution. Acta Crystallogr D 2010;66:213–221.
33. Humphrey W, Dalke A, Schulten K. VMD: Visual molecular dynamics. J Mol Graph 1996;14:33
34. Lindorff-Larsen K, Piana S, Palmo K, Maragakis P, Klepeis JL, Dror RO, Shaw DE. Improved side-chain torsion potentials for the Amber ff99SB protein force field. Proteins 2010;78:1950–1958.
35. Wang JM, Wolf RM, Caldwell JW, Kollman PA, Case DA. Development and testing of a general amber force field. J Comput Chem 2004;25:1157–1174.
36. Nelson MT, Humphrey W, Gursoy A, Dalke A, Kale LV, Skeel RD, Schulten K. NAMD: A parallel, object oriented molecular dynamics program. Int J Supercomput Ap 1996;10:251–268.
37. Harvey MJ, Giupponi G, De Fabritiis G. ACEMD: Accelerating biomolecular dynamics in the microsecond time scale. J Chem Theory Comput 2009;5:1632–1639.
38. Gautieri A, Vesentini S, Redaelli A, Ballarini R. Modeling and measuring visco-elastic properties: From collagen molecules to collagen fibrils. Int J Nonlin Mech 2013;56:25–33.
39. Vesentini S, Redaelli A, Gautieri A. Nanomechanics of collagen microfibrils. Muscles Ligaments Tendons J 2013;3:23–34.
40. Chovancova E, Pavelka A, Benes P, Strnad O, Brezovsky J, Kozlikova B, Gora A, Sustr V, Klvana M, Medek P, Biedermannova L, Sochor J, Damborsky J. CAVER 3.0: A Tool for the analysis of transport pathways in dynamic protein structures. Plos Comput Biol 2012;8: e1002708.
41. Ludemann SK, Lounnas V, Wade RC. How do substrates enter and products exit the buried active site of cytochrome P450cam? 1. Random expulsion molecular dynamics investigation of ligand access channels and mechanisms. J Mol Biol 2000;303:797–811.
42. Barducci A, Bussi G, Parrinello M. Well-tempered metadynamics: A smoothly converging and tunable free-energy method. Phys Rev Lett 2008;100:020603.
43. Bonomi M, Branduardi D, Bussi G, Camilloni C, Provasi D, Raiteri P, Donadio D, Marinelli F, Pietrucci F, Broglia RA, Parrinello M. PLUMED: A portable plugin for free-energy calculations with molecular dynamics. Comput Phys Commun 2009;180:1961–1972.
44. Gilson MK, Given JA, Bush BL, McCammon JA. The statistical-thermodynamic basis for computation of binding affinities: A critical review. Biophys J 1997;72:1047–1069.
45. Lu ND, Kofke DA, Woolf TB. Improving the efficiency and reliability of free energy perturbation calculations using overlap sampling methods. J Comput Chem 2004;25:28–39.
46. Ge X, Roux B. Calculation of the standard binding free energy of sparsomycin to the ribosomal peptidyl-transferase P-site using molecular dynamics simulations with restraining potentials. J Mol Recogn 2010;23:128–141.
47. Fiorin G, Klein ML, Hénin J. Using collective variables to drive molecular dynamics simulations. Mol Phys 2013;111:3345–3362.
48. Wang J, Deng Y, Roux B. Absolute binding free energy calculations using molecular dynamics simulations with restraining potentials. Biophys J 2006;91:2798–2814.
49. Deng Y, Roux B. Computations of standard binding free energies with molecular dynamics simulations. J Phys Chem B 2009;113:1–30.
50. Woo HJ, Roux B. Calculation of absolute protein-ligand binding free energy from computer simulations. Proc Natl Acad Sci 2005; 102:6825–6830.
51. Gumbart JC, Roux B, Chipot C. Standard binding free energies from computer simulations: What is the best strategy? J Chem Theory Comput 2013;9:794–802.
52. Ge X, Roux B. Absolute binding free energy calculations of sparsomycin analogs to the bacterial ribosome. J Phys Chem B 2010;114: 9525–9530.
53. Grandhee SK, Monnier VM. Mechanism of pentosidine formation. Abstr Pap Am Chem S 1991;201:68.Carb.
54. Luers L, Rysiewski K, Dumpitak C, Birkmann E. Kinetics of advanced glycation end products formation on bovine serum albumin with various reducing sugars and dicarbonyl compounds in equimolar ratios. Rejuv Res 2012;15:201–205.
55. Vhangani LN, Van Wyk J. Antioxidant activity of Maillard reaction products (MRPs) derived from fructose–lysine and ribose–lysine model systems. Food Chem 2013;137:92–98.
56. Sievers F, Wilm A, Dineen D, Gibson TJ, Karplus K, Li WZ, Lopez R, McWilliam H, Remmert M, Soding J, Thompson JD, Higgins DG. Fast, scalable generation of high-quality protein multiple sequence alignments using Clustal Omega. Mol Syst Biol 2011;7.:
57. Robert X, Gouet P. Deciphering key features in protein structures with the new ENDscript server. Nucleic Acids Research 2014;42:W320–W324.
58. Hirokawa K, Gomi K, Bakke M, Kajiyama N. Distribution and properties of novel deglycating enzymes for fructosyl peptide in fungi. Arch Microbiol 2003;180:227–231.
59. Kim S, Miura S, Ferri S, Tsugawa W, Sode K. Cumulative effect of amino acid substitution for the development of fructosyl valine-specific fructosyl amine oxidase. Enzyme Microb Tech 2009;44:52–56.
60. Sakaue R, Hiruma M, Kajiyama N, Koyama Y. Cloning and expression of fructosyl-amino acid oxidase gene from Corynebacterium sp 2-4-1 in Escherichia coli. Biosci Biotech Bioch 2002;66: 1256–1261.
61. Yoshida N, Sakai Y, Isogai A, Fukuya H, Yagi M, Tani Y, Kato N. Primary structures of fungal fructosyl amino acid oxidases and their

application to the measurement of glycated proteins. Eur J Biochem 1996;242:499–505.
62. Fujiwara M, Sumitani J, Koga S, Yoshioka I, Kouzuma T, Imamura S, Kawaguchi T, Arai M. Alteration of substrate specificity of fructosyl-amino acid oxidase from Ulocladium sp JS-103. J Biosci Bioeng 2006;102:241–243.
63. Miura S, Ferri S, Tsugawa W, Kim S, Sode K. Development of fructosyl amine oxidase specific to fructosyl valine by site-directed mutagenesis. Protein Eng Des Sel 2008;21:233–239.
64. Fujiwara M, Sumitani J, Koga S, Yoshioka I, Kouzuma T, Imamura S, Kawaguchi T, Arai M. Alteration of substrate specificity of fructosyl-amino acid oxidase from Fusarium oxysporum. Appl Microbiol Biot 2007;74:813–819.
65. Miura S, Ferri S, Tsugawa W, Kiin S, Sode K. Active site analysis of fructosyl amine oxidase using homology modeling and site-directed mutagenesis. Biotechnol Lett 2006;28: 1895–1900.
66. Wu XL, Palfey BA, Mossine VV, Monnier VM. Kinetic studies, mechanism, and substrate specificity of amadoriase I from Aspergillus sp. Biochemistry 2001;40:12886–12895.
67. Miller AG, Hegge S, Uhlmann A, Gerrard JA. A continuous enzyme assay and characterisation of fructosyl amine oxidase enzymes (EC 1.5.3). Arch Biochem Biophys 2005;434:60–66.
68. Wu XL, Takahashi M, Chen SG, Monnier VM. Cloning of amadoriase I isoenzyme from Aspergillus sp.: Evidence of FAD covalently linked to Cys342. Biochemistry 2000;39:1515–1521.